HHS Public Access

Author manuscript

Nat Med. Author manuscript; available in PMC 2014 October 01.

Published in final edited form as:

Nat Med. 2014 April ; 20(4): 360–367. doi:10.1038/nm.3497.

Tissue mechanics modulate microRNA-dependent PTEN expression to regulate malignant progression

Janna K Mouw[1], **Yoshihiro Yui**[1], **Laura Damiano**[1], **Russell O Bainer**[1], **Johnathan N Lakins**[1], **Irene Acerbi**[1], **Guanqing Ou**[1], **Amanda C Wijekoon**[1], **Kandice R Levental**[2], **Penney M Gilbert**[3], **Yunn-Yi Chen**[4], and **Valerie M Weaver**[1,5,6]

[1]Center for Bioengineering and Tissue Regeneration, Department of Surgery, UCSF, San Francisco, California, USA

[2]Department of Integrative Biology and Pharmacology, The University of Texas Health Science Center at Houston - Medical School, Houston, Texas, USA

[3]Institute of Biomaterials & Biomedical Engineering, University of Toronto, Toronto, Ontario, Canada

[4]Department of Pathology, UCSF, San Francisco, California, USA

[5]Department of Anatomy and Department of Bioengineering and Therapeutic Sciences, Eli and Edythe Broad Center of Regeneration Medicine and Stem Cell Research, and UCSF Helen Diller Comprehensive Cancer Center, UCSF, San Francisco, California, USA

Abstract

Tissue mechanics regulate development and homeostasis and are consistently modified in tumor progression. Nevertheless, the fundamental molecular mechanisms through which altered mechanics regulate tissue behavior and the clinical relevance of these changes remain unclear. We demonstrate that increased matrix stiffness modulates microRNA expression to drive tumor progression through integrin activation of β-catenin and MYC. Specifically, in human and mouse tissue, increased matrix stiffness induced miR-18a to reduce levels of the tumor suppressor PTEN, both directly and indirectly by decreasing levels of HOXA9. Clinically, extracellular matrix stiffness correlated significantly with miR-18a in human breast tumor biopsies. miR-18a expression was highest in basal-like breast cancers in which PTEN and HOXA9 levels were lowest and predicted for poor prognosis in patients with luminal breast cancers. Our findings identify a mechanically-regulated microRNA circuit that can promote malignancy and suggest

[6]Correspondence to: Valerie M. Weaver, Center for Bioengineering and Tissue Regeneration, University of California, San Francisco, 513 Parnassus Avenue, HSE-565, San Francisco, CA 94143, Valerie.Weaver@ucsfmedctr.org, Telephone: (415) 476-3826, Fax: (415) 476-3985.

AUTHOR CONTRIBUTIONS

JKM, YY and LD conducted PyMT and V737N mouse experiments. JKM, ACW and KRL fabricated and conducted experiments with the PA hydrogels. ROB and JKM performed the miRNA and large-scale gene expression analyses. JNL designed and constructed expression constructs and the V737N transgenic mouse. JKM and YY performed immunofluorescence imaging, and GO performed the ImageJ analyses. IA and Hongmei Yu performed AFM measurements. YC aided with pathological breast cancer subtyping. PMG conducted the HOXA9 microarray analysis[25]. VMW and JKM wrote the manuscript with input from all authors.

potential prognostic roles for HOXA9 and miR-18a levels in stratifying patients with luminal breast cancers.

INTRODUCTION

Tumors exhibit altered tissue-level and cell mechanics, including extracellular matrix (ECM) remodeling and stiffening, elevated interstitial pressure and altered mass transport[1]. Experimental models demonstrate that enhancing ECM stiffness promotes malignancy and, conversely, inhibiting matrix stiffening reduces tumor incidence and improves treatment[2–4]. Nevertheless, the molecular mechanisms by which mechanics influence cell behavior to modulate malignancy are poorly understood. Additionally, the clinical consequences of altered biophysical cues to the onset, histopathology and progression of cancer remain unclear.

microRNAs (miRNAs) are post-transcriptional regulators of gene expression that are altered in cancers where they modulate levels of tumor suppressors and oncogenes that regulate cell growth, survival and invasion[5,6]. miRNAs also regulate cell–cell and cell–matrix interactions including integrin-dependent adhesion[7]. Integrin signaling is increased in tumors and reduced when ECM stiffening is prevented, indicating potential functional links between miRNAs and tumor mechanics[2,3]. Indeed, ECM stiffness potentiates TGFβ-induced miRNA-dependent metastasis of malignant mammary epithelial cells (MECs)[8], and shear stress and cyclic stretch induce miRNAs in alveolar epithelial and endothelial cells[9,10]. These results indicate miRNAs are sensitive to mechanical cues.

At the intersection of many pathways involved in malignant transformation is phosphoinositide 3-kinase (PI3K), which is critical for cell growth, survival and invasion[11]. We showed that ECM stiffness directly modulates ErbB receptor dependent PI3K activation and MEC invasion, and PI3K signaling is reduced by inhibiting ECM stiffening *in vivo*, implying molecules that influence PI3K signaling are mechanically regulated[2,3]. As a key negative regulator of PI3K activity, phosphatase and tensin homolog (PTEN) is a tumor suppressor frequently reduced in human cancers[12,13]. Here, we used global profiling to identify a mechanically-regulated miRNA, miR-18a, which targets PTEN, both directly and indirectly by decreasing levels of HOXA9, to promote PI3K-dependent malignancy. Clinically, miR-18a expression predicted clinical outcome in patients with luminal breast cancers.

RESULTS

ECM stiffness modulates microRNA expression in culture and *in vivo*

To identify molecular mechanisms whereby mammary tissue responds to differences in the mechanical microenvironment, we profiled miRNAs expressed in non-malignant MCF-10A human mammary epithelial cells (hMECs) on soft (<400Pa) or stiff (>5kPa) polyacrylamide (PA) gels conjugated with recombinant basement membrane (Fig. 1A, Supplementary Tables 1, 2). Interrogation of differentially-expressed miRNAs showed changes in total and mature miRNAs, and revealed that unprocessed miRNAs were somewhat disproportionately

upregulated by ECM stiffness (two-sided Kolmogorov-Smirnov Test, P=0.040, Supplementary Fig. 1A). *In vivo*, we also observed that miRNAs were similarly regulated by ECM stiffness when we prevented ECM cross-linking and stiffening in PyMT mammary tumors by treating mice with either the lysyl oxidase (LOX) pharmacological inhibitor β-aminopropionitrile or with a specific function-blocking antibody to LOX, indicating that cellular miRNAs are responsive to matrix mechanics (Fig. 1B, Supplementary Tables 3, 4).

We noted that within the pool of differentially-expressed, mature miRNAs in the hMECs cultured on the stiff PA gels, miRNAs belonging to the polycistronic miR-17-92 cluster were consistently induced (Supplementary Table 1)[14]. As the miR-17-92 cluster has been implicated in malignancy, we explored the impact of this cluster on stiffness-mediated malignant transformation[14,15]. Dysregulated expression of the cluster's individual miRNAs can drive malignancy through an imbalance of proliferation, apoptosis and differentiation[15,16]. Importantly, only one specific cluster member, miR-18a, was significantly and consistently increased in response to ECM stiffness (Fig. 1C). Indeed, while the miR-17-92 cluster was upregulated with mouse mammary gland transformation, only miR-18a was significantly inhibited in PyMT tumors when tissue fibrosis and stiffening were reduced through LOX inhibition (Fig. 1D, Supplementary Fig. 3A–3C). As we were interested in identifying stiffness-regulated tumor suppressor pathways, we focused our efforts on delineating the role of miR-18a in the mechanical regulation of malignancy.

We first determined that substrate mechanics robustly and consistently increased miR-18a in several non-malignant and transformed breast cancer cell lines in culture (Supplementary Fig. 1B)[18]. We confirmed that miR-18a induced no detectable changes in cell proliferation or apoptosis, but did increase anchorage-independent colony formation in MCF-10A, MCF-7 and T4-2 cells (Supplementary Fig. 1C, 1D). Orthotopic experiments conducted using PyMT mammary tumor cells injected into the cleared mammary fat pads of FVB hosts revealed that increasing miR-18a levels enhanced growth and final tumor volume, as well as lung metastasis (Fig. 1E, 1F). We also found that antagomiR-mediated knockdown of miR-18a in MCF-7 and T4-2 breast cancer cells compromised their growth and survival in soft agar (Supplementary Fig. 1E)[19]. Indeed, knockdown of miR-18a reduced growth and final tumor volume of PyMT mammary tumor cells injected into the cleared fat pad of FVB mice (Fig. 1G) and inhibited their ability to form lung metastasis in a tail vein assay (Fig. 1H, Supplementary Fig. 1F). These findings identify miR-18a as a mechanically-regulated tumor enhancer.

ECM stiffness promotes malignancy by inducing miR-18a to reduce PTEN and enhance PI3K activity

Putative binding regions for miR-18a were identified in the 3′UTR of the tumor suppressor PTEN (Supplementary Fig. 2A)[20–23]. Reporter assays using the putative wild-type and mutated 3′UTR regions of PTEN confirmed that miR-18a interacts with and inhibits PTEN transcription at two of three predicted sites (Fig. 2A, Supplementary Fig. 2B)[24]. PTEN mRNA was reduced in hMECs grown on a stiff substrate (Fig. 2B). Immunofluorescence and immunoblotting also demonstrated loss of PTEN expression in hMECs grown on a stiff substrate, with remarkably less expression in both the nuclear and cytoplasmic fractions

(Fig. 2C, 2D). PTEN mRNA expression was similarly reduced in stiff mouse mammary tumor tissue and inhibiting stromal stiffening (LOX-i or αLOX) prevented PTEN loss (Fig. 2E, Supplementary Fig. 3D). Finally, we documented an inverse correlation between PI3K activity, indicated by elevated phospho-Akt^{Ser473}, and PTEN protein, without any change in cell proliferation or apoptosis, suggesting ECM stiffness could induce miR-18a to modulate malignant progression of the mammary gland by regulating PTEN (Fig. 2F, Supplementary Fig. 3E–3G).

To directly implicate miR-18a in PTEN modulation, we tested whether antagomiR-mediated knockdown of miR-18a could restore PTEN levels in hMECs grown on a stiff ECM. hMECs expressing an antagomiRs to miR-18a (ant-18a) retained PTEN expression even when grown on a stiff PA gel, as compared to the modest increase observed in hMECs expressing an antagomiR to miR-19b (Fig. 2G). PTEN levels were reduced when miR-18a was ectopically elevated in hMECs cultured on a soft ECM (Fig. 2H). Importantly, PTEN mRNA was increased in PyMT tumors in which miR-18a had been reduced, and we noted a reduction in PTEN mRNA in PyMT tumors in which miR-18a had been increased (Fig. 2I, 2J). These findings demonstrate that ECM stiffness represses PTEN and promotes PI3K-dependent malignant progression of the mammary gland by increasing miR-18a.

ECM stiffness promotes malignancy by inducing miR-18a to reduce HOXA9

miRNAs typically have multiple targets and miRNA target prediction software also identified a putative binding region for miR-18a in the 3′UTR of the homeobox transcription regulator HOXA9 (Supplementary Fig. 2)[20–23]. We previously reported that HOXA9 restricts the malignant behavior of breast cancer cells *in vitro* and *in vivo*, and that HOXA9 levels are reduced in human breast cancers and predict poor patient outcome[25]. Accordingly, we explored the impact of miR-18a on HOXA9.

Reporter assays, using a 3′UTR region of HOXA9 containing the putative miR-18a binding region, confirmed that miR-18a interacts with and inhibits HOXA9 expression, and showed that mutating this domain ablates this regulation (Fig. 3A). Consistently, immunoblotting demonstrated significant loss of HOXA9 protein expression in hMECs grown on a stiff substrate, with no change in the mRNA (Fig. 3B, 3C). Immunofluorescence analysis showed robust co-staining of HOXA9 and PTEN only in mammary cells grown on soft ECM and a concomitant loss of both proteins when hMECs were grown on a stiff ECM (Fig. 3D). Moreover, immunofluorescence staining of mammary tissues detected high levels of HOXA9 in normal mammary tissue and showed that, while this expression was lost in the stiffened mammary tumor tissue, inhibiting tissue stiffness tempered the loss of HOXA9, with little effect on mRNA expression (Fig. 3E, 3F, Supplementary Fig. 3D, 3E). These data suggest that miR-18a could also regulate mammary malignancy by regulating HOXA9.

To directly implicate miR-18a in HOXA9 modulation, we tested whether antagomiR-mediated knockdown of miR-18a could restore HOXA9 levels in hMECs grown on a stiff ECM. Consistently, hMECs expressing an antagomiR to miR-18a retained HOXA9 expression even when grown on a stiff PA gel (Fig. 3G). Moreover, HOXA9 levels were reduced when miR-18a was ectopically elevated in hMECs cultured on a soft ECM (Fig. 3H). We also observed an increase in HOXA9 mRNA in PyMT tumors in which miR-18a

had been knocked down and PTEN was restored, and a reduction in HOXA9 mRNA in PyMT tumors in which miR-18a had been increased and PTEN reduced (Fig 3I, 3J). These findings imply a coordinate regulation of HOXA9 and PTEN by miR-18a, suggesting that ECM stiffness promotes malignancy by inducing miR-18a to reduce HOXA9 and PTEN.

ECM stiffness promotes malignancy by preventing HOXA9-dependent PTEN transcription

Our previously published microarray results suggested HOXA9 induced PTEN in breast cancer cells[25]. Consistent with this predicted link between HOXA9 and PTEN, we noted that shRNA-mediated reduction of HOXA9 resulted in a significant loss of PTEN mRNA, even when nonmalignant hMECs were grown on a soft ECM where PTEN levels are elevated (Fig. 4A). Furthermore, increasing levels of HOXA9, using a plasmid lacking a 3′UTR, restored PTEN levels in nonmalignant hMECs grown on a stiff ECM and increased PTEN mRNA levels in two breast cancer cell lines (Fig. 4B, 4C). Moreover, ectopic expression of Hoxa9 in PyMT tumor cells orthotopically-injected into FVB mice increased PTEN mRNA expression and reduced growth and final tumor volume without affecting miR-18a levels (Fig. 4D–4F). These findings indicate that HOXA9 modulates mammary tumorigenesis by regulating PTEN.

Reporter assays, using the proximal promoter region of PTEN[26,27] containing homeobox consensus binding sites, confirmed that luciferase activity was enhanced after co-transfection with increasing amounts of a wild-type but not a DNA binding domain mutant N255T HOXA9 (DNA BM) or by HOXA10 (Fig. 4G, 4H) and that HOXA9 induces PTEN expression independent of the HOX cofactors PBX1 and MEIS1 (Fig. 4I). ChIP studies conducted using endogenous HOXA9 as the bait (in MECs grown on soft ECMs where they express high levels of HOXA9 protein) confirmed that HOXA9 directly binds to the PTEN promoter (Fig. 4J left). This effect was dramatically decreased when HOXA9 levels were reduced via shRNA (Fig. 4J right). The findings indicate that HOXA9 directly binds to the PTEN promoter to regulate its expression and inhibit malignancy of breast cells. The results also demonstrate that increasing mechanical stiffness represses PTEN expression both directly via miR-18a targeting and indirectly via miR-18a targeting of HOXA9 (Fig. 4K).

Tissue stiffness engages mechanotransduction signaling pathways to promote miR-18a dependent malignancy

miRNAs exhibit differential expression across breast cancer subtypes[28], with both tumor initiation and progression regulated by MYC proto-oncogene stimulation of the miR-17-92 cluster[29]. We therefore hypothesized that MYC-driven miRNA expression could be distinctly controlled by the mechanical microenvironment. Both MYC mRNA and protein levels increased with substrate stiffness for non-malignant and malignant hMECs (Fig. 5A, 5B, Supplementary Fig. 4A). Functional linking between MYC expression and mechanics was revealed by showing that pharmacological inhibition of MYC in hMECs cultured on a stiff substrate reduced miR-18a (Fig. 5C). MYC mRNA expression was increased in mouse mammary tumors (Tumor) compared to wild-type glands (and LOX inhibition reduced both mRNA and protein expressions relative to untreated tumors (Fig. 5D) despite similar levels of cell proliferation (Supplementary Fig. 1C, 3F, 3G). These results suggest that MYC is

upregulated by increasing matrix stiffness in culture and *in vivo*, at both the mRNA and protein levels.

Previous work established MYC as a downstream target of β-catenin signaling[31]. Consistently, nuclear β-catenin levels were increased in hMECs grown on stiff substrates (Supplementary Fig. 4B) and the ratio of activated to total β-catenin protein increased with substrate stiffness (Fig. 5E left, Supplementary Fig. 4C). Immunofluorescence also revealed that ECM stiffness increased total nuclear β-catenin (Fig. 5E right). Moreover, nuclear localization of total β-catenin and β-catenin activation were reduced in glands with LOX inhibited compared to control PyMT tumors (Fig. 5F, Supplementary Fig. 4D, 4E).

In both the culture and *in vivo* models, β-catenin mRNA levels were unchanged by ECM stiffness (Supplementary Fig. 4F). However, FAK^{Y397} phosphorylation (indicating FAK activation), GSK3α/β phosphorylation (indicating GSK3 inactivation) and Akt^{S473} phosphorylation (indicating Akt activity) increased with stiffness, suggesting integrin-dependent signaling activates β-catenin (Fig. 5G, Supplementary Fig. 3G, 5A, 5B). Consistently, inhibiting FAK reduced miR-18a expression and increased HOXA9 and PTEN protein expressions (Fig. 5H, 5I). Additionally, inhibition of miR-18a reduced both GSK3α/β and Akt phosphorylation in hMECs cultured on stiff substrates (Supplementary Fig. 5C, 5D). These data demonstrate that tissue stiffening modulates miRNA-dependent PTEN expression through integrin-dependent activation of β-catenin and MYC.

To facilitate integrin clustering *in vivo*, transgenic mice expressing a conditional V737N β1 integrin clustering mutant, which recapitulates tension-dependent integrin clustering and promotes focal adhesion signaling[2], were bred with a mammary gland specific MMTV-Cre transgenic line. Consistent with enhancement of focal adhesion assembly and signaling, FAK^{397} phosphorylation increased in the mutant V737N glands (Fig. 5J). β-catenin nuclear localization was also increased in the mammary epithelium of the V737N glands (Fig. 5K), as were MYC mRNA and miR-18a levels (Fig. 5L). Compellingly, HOXA9 mRNA and protein expressions were inversely correlated with miR-18a in normal and V737N mutant mammary glands (Fig. 5M, Supplementary Fig. 5E). Finally, PTEN mRNA and protein expressions were reduced in the V737N mammary glands compared to WT controls (Fig. 5M, Supplementary Fig. 5F). These results indicate that the mechanical microenvironment influences PTEN expression downstream of integrin activation of β-catenin signaling.

Breast malignancy associates with increased miR-18a and reduced PTEN expression

The clinical relevance of ECM stiffness-induced miR-18a and PTEN repression was investigated by assessing RNA and protein expressions of HOXA9 and PTEN in cohorts of clinically diverse human breast cancers and normal tissue. miR-18a expression was notably higher in breast cancer patient samples compared to normal, with expression in either basal-like or luminal B samples significantly higher than in either normal or luminal A samples (Fig. 6A). miR-18a expression correlated with breast stiffness in both normal and transformed breast tissue (R^2=0.7197, P<0.001, Fig. 6B), with luminal B samples stiffer than luminal A samples (Fig. 6C). PTEN and HOXA9 mRNA were reduced in luminal B cancers compared to normal breast tissue, and further reduced in basal-like cancers (Fig. 6D). Indeed, HOXA9 correlated with PTEN in normal and transformed breast tissue for both

mRNA (R^2=0.8979) and protein, consistent with our findings that PTEN is regulated by HOXA9 (Fig. 6E, 6F). The epithelium of the normal breast co-expressed appreciable quantities of nuclear HOXA9 and cytoplasmic PTEN proteins, as did the more differentiated luminal A breast tumors (Fig. 6F). In contrast, the less differentiated luminal B, basal-like and $HER2^+$ tumors showed reduced expression levels of HOXA9 and PTEN, and higher levels of activated AKT (pAKT substrate), phospho-S6 and inactivated pGSK3 (Fig. 6F, Supplementary Fig 6A). These clinical findings, together with our experimental data, are consistent with the notion that miR-18a and HOXA9 modulate PTEN expression by cooperating with multiple negative and positive regulatory factors differentially expressed in human breast tumors[13].

We next analyzed publicly available gene expression data sets to look for associations between miR-18a and clinical outcome[32,33]. In patient samples without mutations in PTEN, we found that the expression of PTEN correlated with miR-18a expression, but only if HOXA9 was unmethylated (P<0.0001, Supplementary Fig. 6B). We found that miR-18a inversely correlated with time to distant relapse-free survival (DRFS) in patients whose tumors expressed the highest miR-18a levels at initial diagnosis (highest quartile) and experienced distant metastases as a second event, regardless of subtype (P=0.0173, Supplementary Fig. 6C). Including multiple PTEN-targeting miRNAs in two different models, we found that miR-18a expression levels were predictive of outcome among patients with luminal breast cancers (p=0.017 and p=0.049, Fig. 6G, Supplementary Fig. 6D). These data showed that miR-18a is upregulated in basal-like breast cancers and its expression correlates with increased future disease aggression for patients with luminal breast cancers. Combined, these findings identify a mechanically-regulated molecular circuit that may promote malignancy and suggest that matrix stiffness could influence breast cancer pathogenesis (Fig. 6H).

DISCUSSION

Here, we demonstrate that miRNA expression is responsive to ECM stiffness. We present *in vitro* and *in vivo* evidence to show that one miRNA, miR-18a, mediates stiffness-dependent malignancy of breast epithelium. By demonstrating that elevated ECM stiffness engages a miR-18a circuit that promotes PI3K-dependent malignant progression by targeting the tumor suppressor PTEN directly and indirectly via a tumor modifier HOXA9, we established miRNAs as key mediators of tumor mechanics. Given that tissue mechanics are often altered in tumors, our findings provide a plausible explanation for the frequent alteration of miRNA expression across multiple cancer types[6]. Indeed, integrin adhesions and ion channel activity are central players in mechanotransduction that are altered in malignancy and regulated by miRNAs[7,34,35]. Importantly, ECM stiffness is one of multiple aspects of tissue mechanics, which also compromises tissue architecture, interstitial pressure and mass transport, and these physical cues also influence miRNA expression, thereby reinforcing the concept that miRNAs are part of a force-regulated signaling network[1,38–40].

Ultrasound and shear wave elastography interrogate tissue stiffness as a passive feature to detect cancer[41–43]. Yet, studies in experimental models argue that tissue mechanics plays more than just a passenger role in tumor progression[2,3,38]. In patient biopsies, our data

indicate that miR-18a levels can distinguish luminal A from luminal B tumors, and predict clinical outcome in patients with luminal type breast cancer. Our studies are consistent with elastography data on breast cancer patients suggesting that macro-level tumor stiffness may parallel aggression, with tumor size, grade and subtype as independent factors influencing tissue mechanics[42–44]. We extend these observations to show that ECM stiffness can engage a specific molecular pathway, miR-18a regulation of PTEN and HOXA9, which could be clinically exploited. In this regard, luminal breast cancers vary heterogeneously in terms of gene expression, mutations, copy number changes and patient outcome and present a major challenge to identify patients with aggressive versus indolent tumors[33,45,46]. Our work identifies ECM stiffness as a biophysical parameter that can distinguish luminal A from luminal B tumors with miR-18a, PTEN and HOXA9 presenting as tractable biomarkers.

METHODS

Antibodies and Reagents

Antibodies and reagents were as follows: PTEN (Cell Signaling), HOXA9 for immunofluorescence (a gift from T. Nakamura, Japanese Foundation for Cancer Research, Tokyo, Japan), HOXA9 for western blotting (Santa Cruz), phospho-Akt^{Ser473} (Cell Signaling), β-actin (Sigma), Gapdh (Cell Signaling), MYC (Abcam), active b-catenin (Cell Signaling), total β-catenin (Cell Signaling), phospho-GSK3α/β (Cell Signaling), phospho-FAK^{Tyr397} (Invitrogen), phospho-Histone H3 (Cell Signaling), secondary AlexaFluor goat anti-mouse and anti-rabbit (Invitrogen) and Matrigel recombinant basement membrane (BD Biosciences). Inhibitors include MYC inhibitor 10058-F4 (10μM, Calbiochem) and FAK Inhibitor 14 (1μM, Tocris).

Polyacrylamide Substrates and Cell Manipulations

The HMT-3522 S-1 and T4-2 MECs were grown and manipulated as described previously[47,48]. MCF-10A and MDA-MB-231 cells were cultured according to manufacturer's recommendations (ATCC)[2]. BM-conjugated polyacrylamide hydrogels were prepared as previously described[49] with one modification: N-Succinimidyl Acrylamidohexanoic Acid (N6) crosslinker was conjugated to polyacrylamide substrates using 0.01% Bis-acrylamide, 0.025% Irgacure 2959, and 0.002% Di(trimethylolpropane) tetracrylate (Sigma), and 0.01% N6. Soft agar assays were performed as previously described[25].

Vector Constructs and Gene Expression

The β1 integrin wild-type, β1 integrin glycan wedge constitutively active, and β1 integrin clustering mutant V737N constructs have been described[2]. miR-18a, antagomiR-18a and antagomiR-19b constructs, as well as miRNA and antagomiR control constructs, have been previously described[19,50].

Mice and Treatments

FVB/N and FVB/N-Tg (MMTV-PyMT) mice (Jackson Laboratory) were maintained in accordance with University of California Institutional Animal Care and Use Committee guidelines. To generate the FVB/N-Tg (MMTV-V737N) mice, the V737N mutation of the

β1 integrin was cloned downstream of a floxed neomycin phosphotransferase expression cassette in a ROSA 26 targeting construct. Transgenic mice expressing the conditional V737N integrin β1 clustering mutant were bred with the mammary gland specific MMTV-Cre transgenic to generate the FVB/N-Tg (MMTV-V737N) mice (age, 6 weeks; n=6 per group). For LOX-inhibition studies, animals were treated with BAPN (3 mg/kg; Spectrum) in the drinking water (n=10 per group) or a LOX function-blocking polyclonal antibody (3 mg/kg; OpenBiosystems, D8746) injected intraperitoneally twice per week (n=5 per group). Treatment started at 4 weeks and mice were sacrificed after 11 weeks. Lesions were detected by palpation and tumor volume was assessed with calipers. At sacrifice, mammary glands were excised, imaged, and snap frozen or paraformaldehyde-fixed.

For orthotopic injection studies, primary PyMT tumor cells were isolated from PyMT tumors (age, 11 weeks). 1×10^6 primary cells ectopically-expressing miR-18a (n=6 per group), an antagomiR to miR-18a (ant-18a, n=5 per group), Hoxa9 (n=5 per group) or respective appropriate controls were injected into #4 mammary fatpads of 6–7 week old host FVB mice. Mice were sacrificed when tumors reached 1–2cm. Lesions were detected by palpation and tumor volume was assessed with calipers. At sacrifice, tumors were excised, imaged, and snap frozen or paraformaldehyde-fixed. For tail vein studies, primary PyMT tumor cells were isolated from PyMT tumors (age, 11 weeks). 5×10^5 primary cells ectopically-expressing an antagomiR to miR-18a (ant-18a) or an antagomiR control (ant-CTL) were suspended in PBS, and injected into the tail veins of 6–7 week old host FVB mice (n=6 per group). Mice were sacrificed after 28 days. Metastatic burden was assessed by wet lung weight.

miRNA Arrays and Quantitative PCR

Affymetrix miRNA labeling, array hybridization and data pre-processing were performed as previously described[51]. For hMECs microarray experiments, two to four independent experiments were performed under identical conditions. For *in vivo* microarray experiments, n=4 per group. Data were extracted from the images, quantile-normalized, summarized (median polish) and log2-transformed with the miRNA QC tool software from Affymetrix. For miRNA quantitative PCR analysis, reverse transcription of specific miRNAs (from 10ng of total RNA) was carried out using the RT-loop primers for each type of microRNA and the TaqMan microRNA RT kit from Applied Biosystems, according to instructions. cDNA obtained from this step was used to do real-time, quantitative TaqMan PCR using the real-time primers provided, according to instructions. Ct values were converted to fold expression changes ($2^{-\Delta\Delta Ct}$ values) following normalization to U6 snRNA, RNU48 or sno202. For the identification of target miRNAs, attention was focused on miRNAs upregulated in hMECs cultured in a stiff microenvironment, upregulated in the mammary glands of PyMT mice (compared to non-malignant FVB mammary glands), and reduced in LOX-inhibited PyMT mammary glands (compared to control PyMT glands). Additionally, previous work suggests that the most abundant microRNAs in a cell mediate target suppression[52]. miRNA abundance was estimated in the microarray analyses as presented in Tables 1 and 2.

For mRNA analysis, total RNA was reverse transcribed using random primers (Amersham Biosciences), and GAPDH or 18S primers were used to control for cDNA concentration in a separate PCR reactions for each sample. LightCycler Fast Start DNA Master SYBR Green Mix (Roche) was added to each PCR reaction along with cDNA and 1pmol primer in a total volume of 10μl.

Atomic Force Microscopy

Atomic force microscopy and analysis were performed using an MFP3D-BIO inverted optical atomic force microscope mounted on a Nikon TE2000-U inverted fluorescent microscope (Asylum Research) as previously described[53].

Immunostaining, Immunoblot, ChIP and Reporter Assays

Immunofluorescence imaging of cultures and tissues was performed as described[2]. Cells were lysed in RIPA or Laemmli buffer and assayed by immunoblotting[54]. Chromatin immunoprecipitation assays were performed as previously described[25]. Luciferase reporter assays were quantified by SEAP expression, and were performed as previously described[24,25]. For the V737N β-catenin nuclear localization analysis shown in Fig. 5J, β-catenin and DAPI co-localization was determined via ImageJ, and non-nuclear β-catenin has been removed from the images displayed.

Human samples

Breast cancer subtypes were approximated using defined clinicopathological criteria[55,56]. Briefly, luminal A tumors are defined as ER and/or PR positive, HER2 negative, Ki-67 low (<14%); luminal B tumors as ER and/or PR positive, HER2 negative and Ki-67 high (or any Ki-67 status and HER2 amplified); basal-like tumors as ER and PR negative, HER2 not overexpressed or amplified; and HER2-overexpressing tumors as ER and PR negative, HER2 overexpressed or amplified.

Formalin-fixed, paraffin-embedded human breast tissue sections and freshly isolated RNA, lacking any patient-identifying information, were obtained with IRB approval from the University of California, San Francisco with patient consent or commercially (Biomax or OriGene). Immunofluorescence was performed as previously described[25]. For miRNA and mRNA assays, 15 non-malignant, 25 luminal A, 25 luminal B, 25 basal-like and 15 HER2+ samples were examined. For analyses of paraffin-embedded sections, 10 non-malignant, 20 luminal A, 20 luminal B, 20 basal-like and 35 HER2+ samples were examined.

Bioinformatics

To generate the heatmap images, we estimated the correlation between mRNA and miRNA abundance and patient outcome by calculating pairwise Spearman correlation coefficients between the normalized expression estimates or untransformed DRFS values across all patients as appropriate, and clustered the resulting correlation matrices by Euclidean distance. We related the expression of miR-18a to DRFS in a panel of breast cancers by fitting a multivariate cox regression model to the data[32,33]. In the model, we stratified patients by subtype[55,56] and included independent covariates modeling miR-18a expression, patient age, and tumor size as continuous variables, and tumor grade and lymph node

presence as binary factors. We estimated the significance of the association of each covariate to DRFS in the framework of the regression model using a Wald test to generate *P*-values. We visualized patient survival within each subgroup as Kaplan-Meyer curves by plotting the surviving proportion of patients within the top and bottom quartiles of miR-18a expression as a function of time.

Statistics

Statistical analysis was performed with either an unpaired student's t test, two-way ANOVA, General Linear Model, Fisher's exact test or Mann-Whitney U test (where appropriate). Expression estimates represented in violin plots were analyzed with a Kolmogorov-Smirnov test. We used Minitab software to conduct the statistical analysis of our data. *P*-values of less than 0.05 were considered to be significant.

Supplementary Material

Refer to Web version on PubMed Central for supplementary material.

Acknowledgments

We thank the members of the Weaver and Dr. Nancy Boudreau labs for helpful discussions. AFM analysis of the PyMT samples was performed by Dr. Hongmei Yu at the University of California, San Francisco (San Francisco, CA). Animal handling was supported by Lidiya Korets at the University of California, San Francisco (San Francisco, CA). miRNA and antagomiR constructs were provided by Dr. Michaela Scherr at the Medical School Hannover (Hannover, Germany). PTEN proximal promoter constructs were provided by Dr. Charis Eng at the Genomic Medical Institute (Cleveland, OH). LOX inhibitory antibodies were provided by Dr. Amato Giaccia at the Stanford University School of Medicine (Stanford, CA). This work was supported by DOD BCRP grant W81XWH-07-1-0538 (JKM), Susan G Komen Postdoctoral Fellowship PDF12230246 (IA), DOD BCRP grants W81XWH-05-1-0330 and W81XWH-13-1-0216 (VMW), NIH NCI grants R01 CA138818, U54 CA143836, R01 CA085492 and U01 ES019458 (VMW), and Susan G. Komen grant KG110560PP (VMW).

References

1. Kumar S, Weaver VM. Mechanics, malignancy, and metastasis: the force journey of a tumor cell. Cancer metastasis reviews. 2009; 28:113–27. [PubMed: 19153673]
2. Paszek MJ, et al. Tensional homeostasis and the malignant phenotype. Cancer Cell. 2005 Submitted.
3. Levental KR, et al. Matrix crosslinking forces tumor progression by enhancing integrin signaling. Cell. 2009; 139:891–906. [PubMed: 19931152]
4. Provenzano PP, et al. Enzymatic targeting of the stroma ablates physical barriers to treatment of pancreatic ductal adenocarcinoma. Cancer cell. 2012; 21:418–29. [PubMed: 22439937]
5. Tavazoie SF, et al. Endogenous human microRNAs that suppress breast cancer metastasis. Nature. 2008; 451:147–52. [PubMed: 18185580]
6. Zhang B, Pan X, Cobb GP, Anderson TA. microRNAs as oncogenes and tumor suppressors. Developmental biology. 2007; 302:1–12. [PubMed: 16989803]
7. Valastyan S, Weinberg RA. Roles for microRNAs in the regulation of cell adhesion molecules. Journal of cell science. 2011; 124:999–1006. [PubMed: 21402873]
8. Taylor MA, Sossey-Alaoui K, Thompson CL, Danielpour D, Schiemann WP. TGF-β upregulates miR-181a expression to promote breast cancer metastasis. The Journal of clinical investigation. 2013; 123:150–63. [PubMed: 23241956]
9. Neth P, Nazari-Jahantigh M, Schober A, Weber C. MicroRNAs in flow-dependent vascular remodelling. Cardiovascular research. 2013; 99:294–303. [PubMed: 23612583]
10. Yehya N, Yerrapureddy A, Tobias J, Margulies SS. MicroRNA modulate alveolar epithelial response to cyclic stretch. BMC genomics. 2012; 13:154. [PubMed: 22537220]

11. Krasilnikov MA. Phosphatidylinositol-3 kinase dependent pathways: the role in control of cell growth, survival, and malignant transformation. Biochemistry. Biokhimii_a. 2000; 65:59–67.
12. Hollander MC, Blumenthal GM, Dennis PA. PTEN loss in the continuum of common cancers, rare syndromes and mouse models. Nature reviews. Cancer. 2011; 11:289–301. [PubMed: 21430697]
13. Salmena L, Carracedo A, Pandolfi PP. Tenets of PTEN Tumor Suppression. Cell. 2008; 133:403–414. [PubMed: 18455982]
14. Olive V, Li Q, He L. mir-17-92: a polycistronic oncomir with pleiotropic functions. Immunological reviews. 2013; 253:158–66. [PubMed: 23550645]
15. Li Y, et al. The miR-17-92 cluster expands multipotent hematopoietic progenitors whereas imbalanced expression of its individual oncogenic miRNAs promotes leukemia in mice. Blood. 2012; 119:4486–98. [PubMed: 22451425]
16. Suárez Y, et al. Dicer-dependent endothelial microRNAs are necessary for postnatal angiogenesis. Proceedings of the National Academy of Sciences of the United States of America. 2008; 105:14082–7. [PubMed: 18779589]
17. Colas AR, et al. Whole-genome microRNA screening identifies let-7 and mir-18 as regulators of germ layer formation during early embryogenesis. Genes & development. 2012; 26:2567–79. [PubMed: 23152446]
18. Kenny PA, et al. The morphologies of breast cancer cell lines in three-dimensional assays correlate with their profiles of gene expression. 2007; 1:84–96.
19. Scherr M, et al. Lentivirus-mediated antagomir expression for specific inhibition of miRNA function. Nucleic acids research. 2007; 35:e149. [PubMed: 18025036]
20. John B, et al. Human MicroRNA targets. PLoS biology. 2004; 2:e363. [PubMed: 15502875]
21. Betel D, Koppal A, Agius P, Sander C, Leslie C. Comprehensive modeling of microRNA targets predicts functional non-conserved and non-canonical sites. Genome biology. 2010; 11:R90. [PubMed: 20799968]
22. Betel D, Wilson M, Gabow A, Marks DS, Sander C. The microRNA.org resource: targets and expression. Nucleic acids research. 2008; 36:D149–53. [PubMed: 18158296]
23. Enright AJ, et al. MicroRNA targets in Drosophila. Genome biology. 2003; 5:R1. [PubMed: 14709173]
24. Jin Y, Chen Z, Liu X, Zhou X. Evaluating the microRNA targeting sites by luciferase reporter gene assay. Methods in molecular biology (Clifton, NJ). 2013; 936:117–27.
25. Gilbert PM, et al. HOXA9 regulates BRCA1 expression to modulate human breast tumor phenotype. The Journal of clinical investigation. 2010; 120:1535–50. [PubMed: 20389018]
26. Moens CB, Selleri L. Hox cofactors in vertebrate development. Dev Biol. 2006; 291:193–206. [PubMed: 16515781]
27. Tang Y, Eng C. PTEN autoregulates its expression by stabilization of p53 in a phosphatase-independent manner. Cancer research. 2006; 66:736–42. [PubMed: 16424003]
28. Dvinge H, et al. The shaping and functional consequences of the microRNA landscape in breast cancer. Nature. 2013; 497:378–82. [PubMed: 23644459]
29. Dews M, et al. Augmentation of tumor angiogenesis by a Myc-activated microRNA cluster. Nature genetics. 2006; 38:1060–5. [PubMed: 16878133]
30. Goga A, Yang D, Tward AD, Morgan DO, Bishop JM. Inhibition of CDK1 as a potential therapy for tumors over-expressing MYC. Nature medicine. 2007; 13:820–7.
31. He TC, et al. Identification of c-MYC as a target of the APC pathway. Science (New York, NY). 1998; 281:1509–12.
32. Buffa FM, et al. microRNA-associated progression pathways and potential therapeutic targets identified by integrated mRNA and microRNA expression profiling in breast cancer. Cancer research. 2011; 71:5635–45. [PubMed: 21737487]
33. Comprehensive molecular portraits of human breast tumours. Nature. 2012; 490:61–70. [PubMed: 23000897]
34. Delmas P, Coste B. Mechano-gated ion channels in sensory systems. Cell. 2013; 155:278–84. [PubMed: 24120130]

35. Wang Z. miRNA in the regulation of ion channel/transporter expression. Comprehensive Physiology. 2013; 3:599–653. [PubMed: 23720324]
36. Reddy BVVG, Irvine KD. Regulation of Hippo signaling by EGFR-MAPK signaling through Ajuba family proteins. Developmental cell. 2013; 24:459–71. [PubMed: 23484853]
37. James V, et al. LIM-domain proteins, LIMD1, Ajuba, and WTIP are required for microRNA-mediated gene silencing. Proceedings of the National Academy of Sciences of the United States of America. 2010; 107:12499–504. [PubMed: 20616046]
38. Provenzano PP, Inman DR, Eliceiri KW, Keely PJ. Matrix density-induced mechanoregulation of breast cell phenotype, signaling and gene expression through a FAK-ERK linkage. Oncogene. 2009; 28:4326–43. [PubMed: 19826415]
39. Huang S, Ingber DE. Cell tension, matrix mechanics, and cancer development. Cancer Cell. 2005; 8:175–176. [PubMed: 16169461]
40. Vogel V, Sheetz M. Local force and geometry sensing regulate cell functions. Nature reviews. Molecular cell biology. 2006; 7:265–75. [PubMed: 16607289]
41. Fasching PA, et al. Influence of mammographic density on the diagnostic accuracy of tumor size assessment and association with breast cancer tumor characteristics. European journal of radiology. 2006; 60:398–404. [PubMed: 17030108]
42. Chang JM, et al. Stiffness of tumours measured by shear-wave elastography correlated with subtypes of breast cancer. European radiology. 2013; 23:2450–8. [PubMed: 23673574]
43. Evans A, et al. Quantitative shear wave ultrasound elastography: initial experience in solid breast masses. Breast cancer research_: BCR. 2010; 12:R104. [PubMed: 21122101]
44. Chang JM, et al. Clinical application of shear wave elastography (SWE) in the diagnosis of benign and malignant breast diseases. Breast cancer research and treatment. 2011; 129:89–97. [PubMed: 21681447]
45. Paik S, et al. A multigene assay to predict recurrence of tamoxifen-treated, node-negative breast cancer. The New England journal of medicine. 2004; 351:2817–26. [PubMed: 15591335]
46. Parker JS, et al. Supervised risk predictor of breast cancer based on intrinsic subtypes. Journal of clinical oncology_: official journal of the American Society of Clinical Oncology. 2009; 27:1160–7. [PubMed: 19204204]
47. Wang F, et al. Reciprocal interactions between beta1-integrin and epidermal growth factor receptor in three-dimensional basement membrane breast cultures: a different perspective in epithelial biology. Proc Natl Acad Sci U S A. 1998; 95:14821–14826. [PubMed: 9843973]
48. Weaver VM, et al. Reversion of the malignant phenotype of human breast cells in three-dimensional culture and in vivo by integrin blocking antibodies. J Cell Biol. 1997; 137:231–245. [PubMed: 9105051]
49. Lakins JN, Chin AR, Weaver VM. Exploring the link between human embryonic stem cell organization and fate using tension-calibrated extracellular matrix functionalized polyacrylamide gels. Methods in molecular biology (Clifton, NJ). 2012; 916:317–50.
50. Stegmeier F, Hu G, Rickles RJ, Hannon GJ, Elledge SJ. A lentiviral microRNA-based system for single-copy polymerase II-regulated RNA interference in mammalian cells. Proceedings of the National Academy of Sciences of the United States of America. 2005; 102:13212–7. [PubMed: 16141338]
51. Gan L, Schwengberg S, Denecke B. MicroRNA profiling during cardiomyocyte-specific differentiation of murine embryonic stem cells based on two different miRNA array platforms. PloS one. 2011; 6:e25809. [PubMed: 21991358]
52. Mullokandov G, et al. High-throughput assessment of microRNA activity and function using microRNA sensor and decoy libraries. Nature methods. 2012; 9:840–6. [PubMed: 22751203]
53. Lopez JI, Mouw JK, Weaver VM. Biomechanical regulation of cell orientation and fate. Oncogene. 2008; 27:6981–93. [PubMed: 19029939]
54. Johnson KR, Leight JL, Weaver VM. Demystifying the effects of a three-dimensional microenvironment in tissue morphogenesis. Methods Cell Biol. 2007; 83:547–583. [PubMed: 17613324]
55. Goldhirsch A, et al. Strategies for subtypes--dealing with the diversity of breast cancer: highlights of the St. Gallen International Expert Consensus on the Primary Therapy of Early Breast Cancer

2011. Annals of oncology_: official journal of the European Society for Medical Oncology/ESMO. 2011; 22:1736–47. [PubMed: 21709140]

56. Von Minckwitz G, et al. Response-Guided Neoadjuvant Chemotherapy for Breast Cancer. Journal of clinical oncology_: official journal of the American Society of Clinical Oncology. 2013; 31:3623–3630. [PubMed: 24002511]

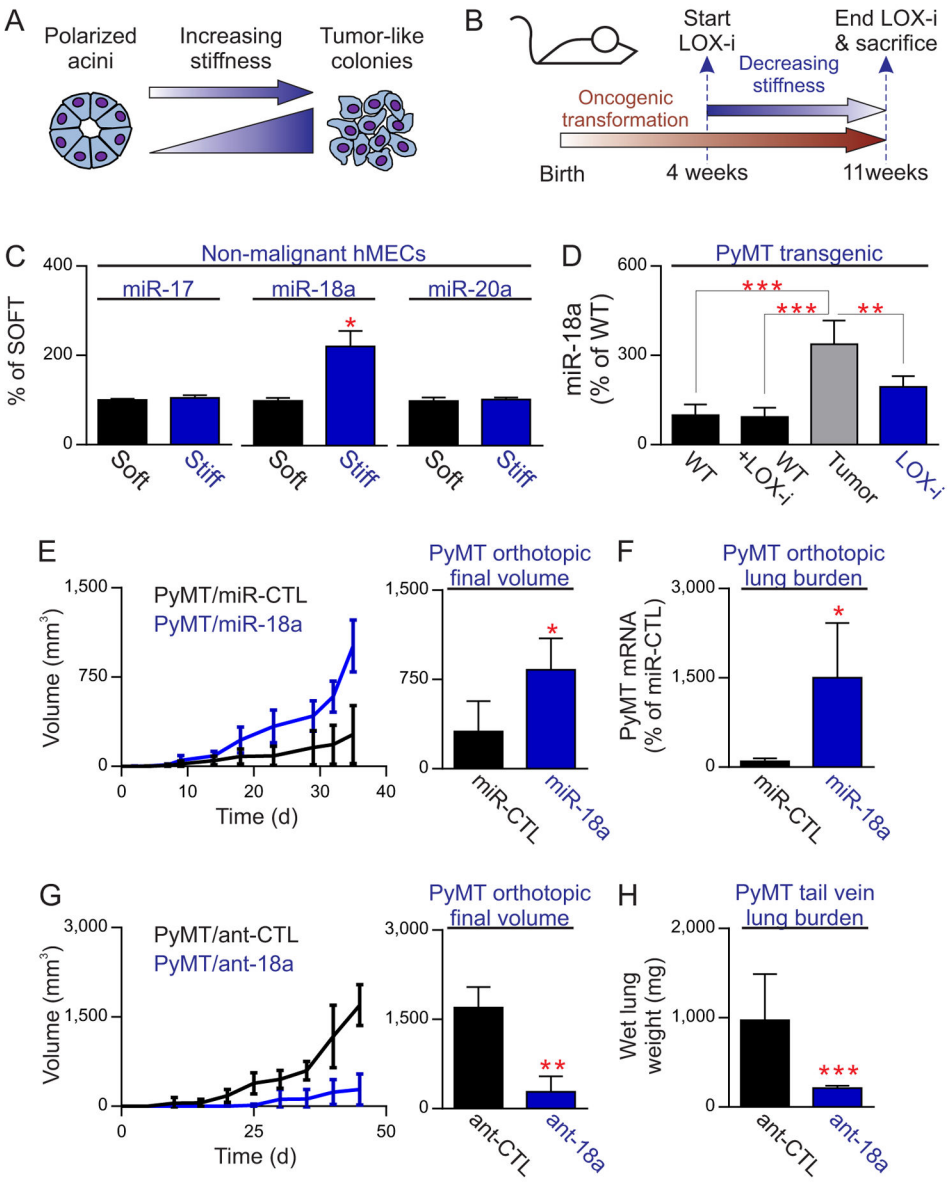

Figure 1. ECM stiffness modulates microRNA expression in culture and *in vivo*

A. Graphic depicting the *in vitro* experimental approach using human mammary epithelial cells (hMECs) and synthetic polyacrylamide (PA) substrates functionalized with recombinant basement membrane (BM) to mimic the mechanical properties of the normal human mammary gland and of mammary tumors during malignant progression. B. Graphic depicting the *in vivo* experimental approach inhibiting LOX using the polyoma middle T (PyMT) mouse model of breast cancer. C. Validation and quantification of miR-17-92 targets (with $P<0.05$ from the microarray results) with qPCR. miRNA targets were normalized with RNU48 and graphed relative to the soft group. D. qPCR of miR-18a for FVB mice (WT), FVB mice treated with a LOX inhibitor (WT+LOX-i), control PyMT mice (Tumor) and PyMT mice treated with a LOX inhibitor (LOX-i, n=10/group). Murine miR targets were normalized with U6 and graphed relative to the FVB (WT) group. E.

Quantification of tumor growth and final tumor volume for PyMT primary tumor cells orthotopically injected into the #4 mammary gland of FVB hosts (n=6/group). PyMT cells expressed either a control construct (miR-CTL) or miR-18a. F. Quantification of PyMT mRNA expression from the lungs of host FVB mice orthotopically injected with PyMT cells expressing either a control construct (miR-CTL) or miR-18a (n=6/group). Results were normalized to 18S and graphed relative to miR-CTL. G. Quantification of tumor growth and final tumor volume for PyMT primary tumor cells orthotopically injected into the #4 mammary gland of FVB hosts (n=5/group). PyMT cells expressed either a control antagomiR (ant-CTL) or an antagomiR to miR-18a (ant-18a). H. Quantification of lung weight for FVB mice tail-vein injected with PyMT primary cells expressing either a control antagomiR (ant-CTL) or an antagomiR to miR-18a (ant-18a, n=6/group). For *in vitro* bar graphs, results are the mean ± S.E.M. of at least 3 independent experiments. For *in vivo* bar graphs, results are the mean ± S.D. (*, $P<0.05$; **, $P<0.01$; ***, $P< 0.001$)

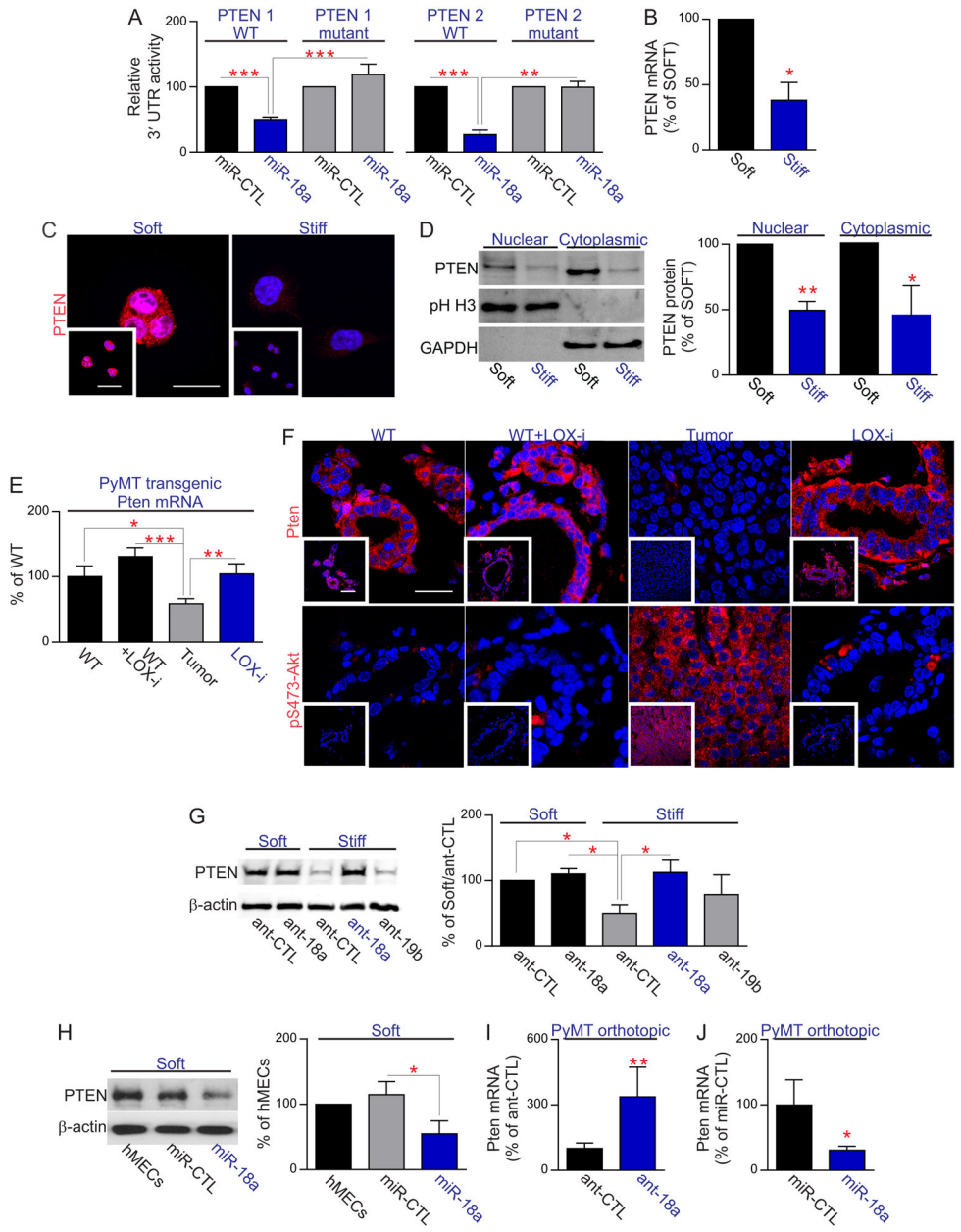

Figure 2. ECM stiffness promotes malignancy by inducing miR-18a to reduce PTEN and enhance PI3K activity

A. Luciferase reporter analysis of either wild-type or mutated PTEN 3′UTR activity (for two putative miRNA seed regions) upon addition of 1μg of either a control (miR-CTL) or miR-18a. Results are normalized to respective miR-CTL groups. B. PTEN mRNA for hMECs cultured on soft (<400Pa) or stiff (>5kPa) PA gels. Results are normalized to 18S and graphed relative to soft. C. Immunofluorescence images for PTEN (red) and DAPI (blue) in hMECs cultured on soft or stiff PA gels. Scale bar, 20μm; inset scale bar, 50μm. D. Nuclear and cytoplasmic PTEN protein for hMECs cultured on soft or stiff PA gels. Results are normalized to pHistone H3 (nuclear) or Gapdh (cytoplasmic), and graphed relative to soft. E. PTEN mRNA for FVB mice (WT), FVB mice treated with a LOX inhibitor (WT

+LOX-i), control PyMT mice (Tumor) and PyMT mice treated with a LOX inhibitor (LOX-i). Results are normalized to 18S and graphed relative to WT (n=10/group). F. Immunofluorescent images of Pten (top, red), pS473-Akt (bottom, red) and DAPI (blue) of mammary glands from FVB mice (WT), FVB mice treated with a LOX inhibitor (WT +LOX-i), malignant PyMT mice (Tumor) and PyMT mice treated with a LOX inhibitor (LOX-i). Scale bar, 20μm; inset scale bar, 50μm. G. PTEN protein expression for hMECs cultured on soft or stiff substrates expressing a microRNA antagomiR control (ant-CTL), an antagomiR to miR-18a (ant-18a) or an antagomiR to miR-19b (ant-19b). Results are normalized to β-actin and graphed relative to soft vector. H. PTEN protein expression for hMECs cultured on soft substrates expressing the control vector (miR-CTL), miR-18a, or without expression vectors (hMECs). Results are normalized to β-actin and graphed relative to hMECs. I. Pten mRNA expression for orthotopic PyMT tumors expressing either a microRNA antagomiR control (ant-CTL) or an antagomiR to miR-18a (ant-18a, n=5/group). Results are normalized to 18S and graphed relative to ant-CTL. J. Pten mRNA expression for orthotopic PyMT tumors expressing either a microRNA control vector (miR-CTL) or miR-18a (n=6/group). Results are normalized to 18S and graphed relative to miR-CTL. In all *in vitro* bar graphs, results are the mean ± S.E.M. of at least 3 independent experiments. For *in vivo* bar graphs, results are the mean ± S.D. (*, $P<0.05$; **, $P<0.01$; ***, $P< 0.001$)

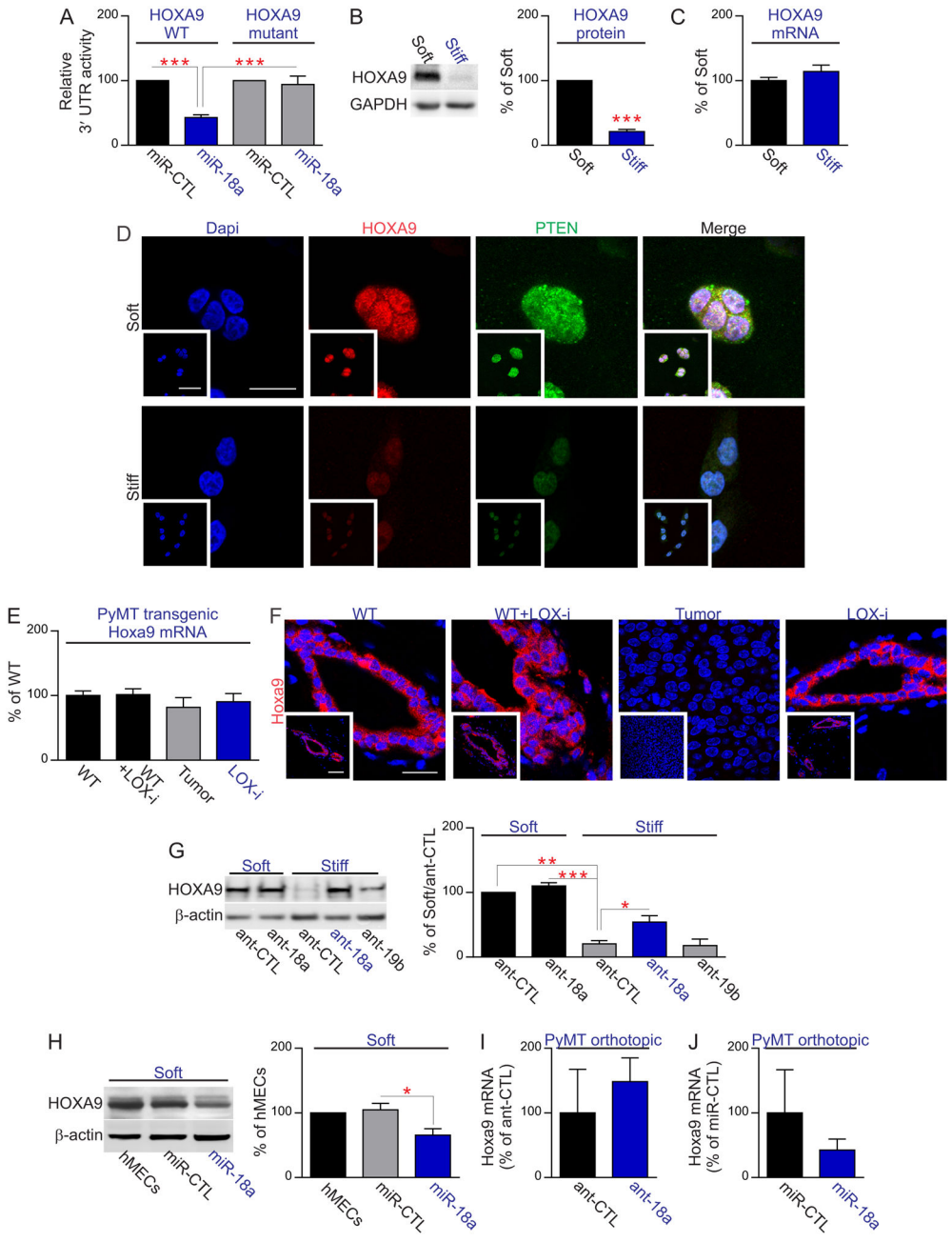

Figure 3. ECM stiffness promotes malignancy by inducing miR-18a to reduce HOXA9

A. Luciferase reporter analysis of either wild-type or mutated HOXA9 3′UTR activity upon addition of 1μg of either a control vector (miR-CTL) or miR-18a. Results are normalized to respective miR-CTL groups. B. HOXA9 protein for hMECs cultured on soft (<400Pa) or stiff (>5kPa) PA gels. Results are normalized to Gapdh and graphed relative to soft. C. HOXA9 mRNA for hMECs cultured on soft or stiff PA gels. Results are normalized to Gapdh and graphed relative to SOFT. D. Immunofluorescence images for HOXA9 (red), PTEN (green) and DAPI (blue) in hMECs cultured on soft or stiff PA gels. Scale bar, 20μm; inset scale bar, 50μm. E. HOXA9 mRNA for FVB mice (WT), control PyMT mice (Tumor)

and PyMT mice treated with a LOX inhibitor (LOX-i). Results are normalized to 18S and graphed relative to WT (n=10/group). F. Immunofluorescence images of HOXA9 (red) and DAPI (blue) for FVB mice (WT), FVB mice treated with a LOX inhibitor (WT+LOX-i), control PyMT mice (Tumor) and PyMT mice treated with a LOX inhibitor (LOX-i). Scale bar, 20μm; inset scale bar, 50μm. G. HOXA9 protein for hMECs cultured on soft or stiff substrates expressing an microRNA antagomiR control, an antagomiR to miR-18a (ant-18a) or an antagomiR to miR-19b (ant-19b). Results are normalized to β-actin and graphed relative to soft vector. H. HOXA9 protein for hMECs cultured on soft substrates expressing the control vector (miR-CTL), miR-18a, or without expression vectors (hMECs). Results are normalized to β-actin and graphed relative to hMECs. I. Hoxa9 mRNA expression for orthotopic PyMT tumors expressing either a microRNA antagomiR control (ant-CTL) or an antagomiR to miR-18a (ant-18a, n=5/group). Results are normalized to 18S and graphed relative to ant-CTL. J. Hoxa9 mRNA expression for orthotopic PyMT tumors expressing either a microRNA control vector (miR-CTL) or miR-18a (n=6/group). Results are normalized to 18S and graphed relative to miR-CTL. In all *in vitro* bar graphs, results are the mean ± S.E.M. of at least 3 independent experiments. For *in vivo* bar graphs, results are the mean ± S.D. (*, $P<0.05$; **, $P<0.01$; ***, $P< 0.001$)

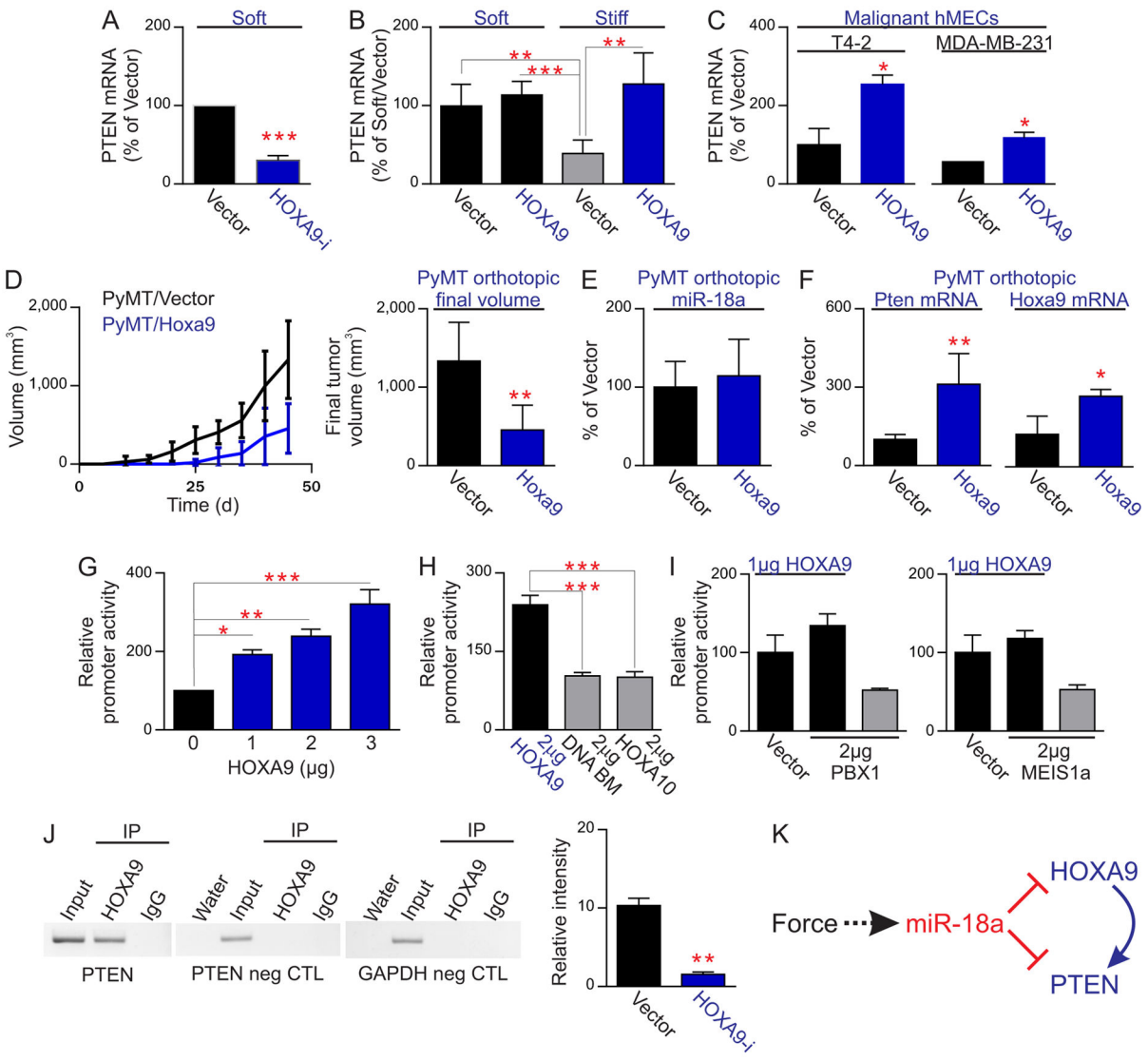

Figure 4. ECM stiffness promotes malignancy by preventing HOXA9-dependent PTEN transcription

A. PTEN mRNA expression in hMECs expressing a control shRNA (Vector) or an shRNA to HOXA9 (HOXA9-i), and cultured on a soft (<400Pa) substrate. Results are normalized to 18S and graphed relative to Vector. B. PTEN mRNA expression in hMECs cultured on a soft (<400Pa) or stiff (>5kPa) substrate, ectopically expressing a control vector (Vector) or HOXA9. Results are normalized to 18S and graphed relative to soft. C. PTEN mRNA expression in malignant hMECs (T4-2 or MDA-MB-231 cells) ectopically expressing a control vector (Vector) or HOXA9. Results are normalized to 18S and graphed relative to soft. D. Quantification of tumor growth and final tumor volume for PyMT primary tumor cells expressing either a control vector (Vector) or Hoxa9, and orthotopically injected into the #4 mammary gland of FVB hosts (n=5/group). E. miR-18a expression for orthotopic PyMT tumors expressing either a control vector (Vector) or Hoxa9 (n=5/group). Results are normalized to 18S and graphed relative to Vector. F. Pten and Hoxa9 expressions for orthotopic PyMT tumors expressing either a control vector (Vector) or Hoxa9 (n=5/group).

Results are normalized to 18S and graphed relative to Vector. G. Luciferase reporter analysis of PTEN promoter activity in response to the addition of wild-type HOXA9. H. Luciferase reporter analysis of PTEN promoter activity upon addition of 2μg HOXA9 containing an N255T (DNA BM) mutation in the conserved DNA binding domain or the addition of 2μg of HOXA10. I. Luciferase reporter analysis of PTEN promoter activity in response to 1μg HOXA9 with 2μg of either PBX1 or MEIS1a. J. Representative gel of ChIP studies in hMECs, revealing co-precipitation of HOXA9 with the PTEN promoter. Quantification of the chromatin immunoprecipitation results of HOXA9 on the PTEN proximal promoter for non-malignant hMECs expressing either a shRNA control (Vector) or an shRNA to HOXA9 (HOXA9-i). K. Graphic depicting a model for suppression of PTEN directly via miR-18a and indirectly through miR-18a regulation of HOXA9. In all *in vitro* bar graphs, results are the mean ± S.E.M. of at least 3 independent experiments. For *in vivo* bar graphs, results are the mean ± S.D. (*, $P<0.05$; **, $P<0.01$; ***, $P< 0.001$)

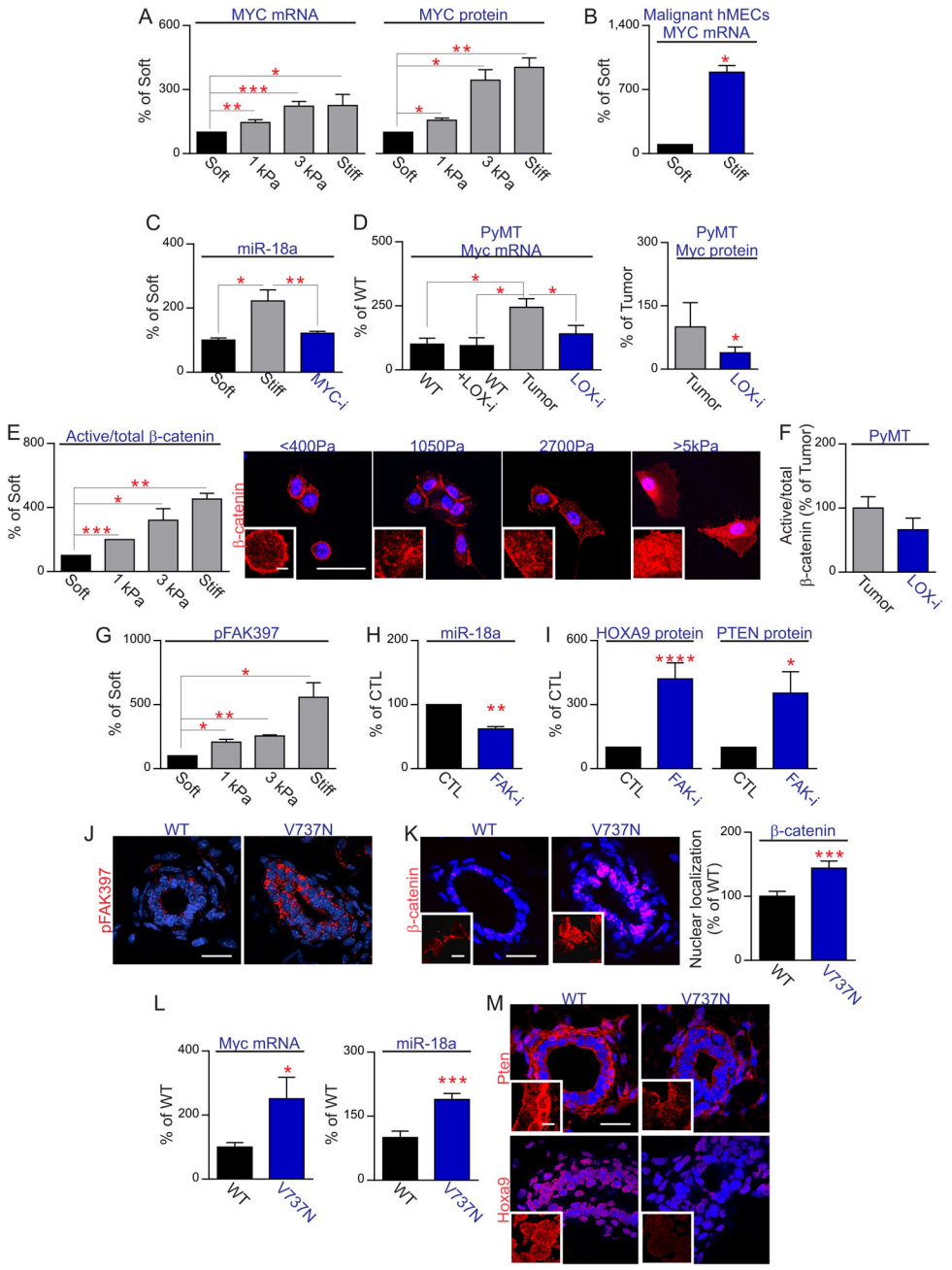

Figure 5. Tissue stiffness engages mechanotransduction signaling pathways to promote miR-18a dependent malignancy

A. MYC mRNA and protein expressions in hMECs cultured on PA gels of increasing stiffness. Results are normalized to GAPDH and graphed relative to soft (<400Pa). B. MYC mRNA expression in malignant T4-2 hMECs cultured on soft (<400Pa) and stiff (>5kPa) PA gels. Results are normalized to GAPDH and graphed relative to soft. C. miR-18a expression for hMECs cultured on a soft substrate (<400Pa), or on a stiff substrate (>5kPa) with 10μM of the MYC inhibitor 10058-F4 (MYC-i). Results are normalized to RNU48 and graphed relative to soft. D. *Left*: Myc mRNA expression in mammary glands from FVB

mice (WT), FVB mice treated with a LOX inhibitor (WT+LOX-i), malignant PyMT mice (Tumor) and PyMT mice treated with a LOX inhibitor (LOX-i). Results are normalized to 18S and graphed relative to WT (n=10/group). *Right*: Myc protein expression in mammary glands from malignant PyMT mice (Tumor) and PyMT mice treated with a LOX inhibitor (LOX-i). Results are graphed relative to Tumor (n=5/group). E. *Left*: Active β-catenin protein expression normalized to total β-catenin, in hMECs cultured on PA gels of increasing stiffness. Results are normalized to total β-catenin and graphed relative to soft. *Right*: Immunofluorescence images of β-catenin (red) and DAPI (blue) in hMECs cultured on PA gels of increasing stiffness. Scale bar, 50μm; inset scale bar, 5μm. F. Active β-catenin protein expression normalized to total β-catenin in mammary glands from malignant PyMT mice (Tumor) and PyMT mice treated with a LOX inhibitor (LOX-i). Results are graphed relative to Tumor (n=5/group). G. $pFAK^{397}$ protein expression in hMECs cultured on PA gels of increasing stiffness. Results are normalized to GAPDH and graphed relative to soft. H. miR-18a expression for hMECs cultured on a stiff substrate (>5kPa) with and without 1μM of the FAK inhibitor, FAK inhibitor 14 (FAK-i). Results are normalized to RNU48 and graphed relative to CTL (no inhibitor). I. HOXA9 and PTEN protein expressions for hMECs cultured on a stiff substrate (>5kPa) with and without 1μM of FAK inhibitor 14 (FAK-i). Results are normalized to GAPDH and graphed relative to CTL (no inhibitor). J. Immunofluorescence images of $pFAK^{Y397}$ (red) and DAPI (blue) in FVB (WT) and transgenic V737N mice (n=6/group). Scale bar, 20μm. K. β-catenin nuclear expression in FVB (WT) and transgenic V737N mice (n=6/group). Results are normalized to total β-catenin expression and graphed relative to WT. Scale bar, 20μm; inset scale bar, 5μm. L. Myc mRNA and miR-18a expressions in FVB (WT) and transgenic V737N mice (n=6/group). Results are normalized to 18S and sno202 respectively, and graphed relative to WT. M. Pten and Hoxa9 protein expressions in FVB (WT) and transgenic V737N mice (n=6/group). Scale bar, 20μm; inset scale bar, 5μm. In all *in vitro* bar graphs, results are the mean ± S.E.M. of at least 3 independent experiments. For *in vivo* bar graphs, results are the mean ± S.D. (*, $P<0.05$; **, $P<0.01$; ***, $P< 0.001$)

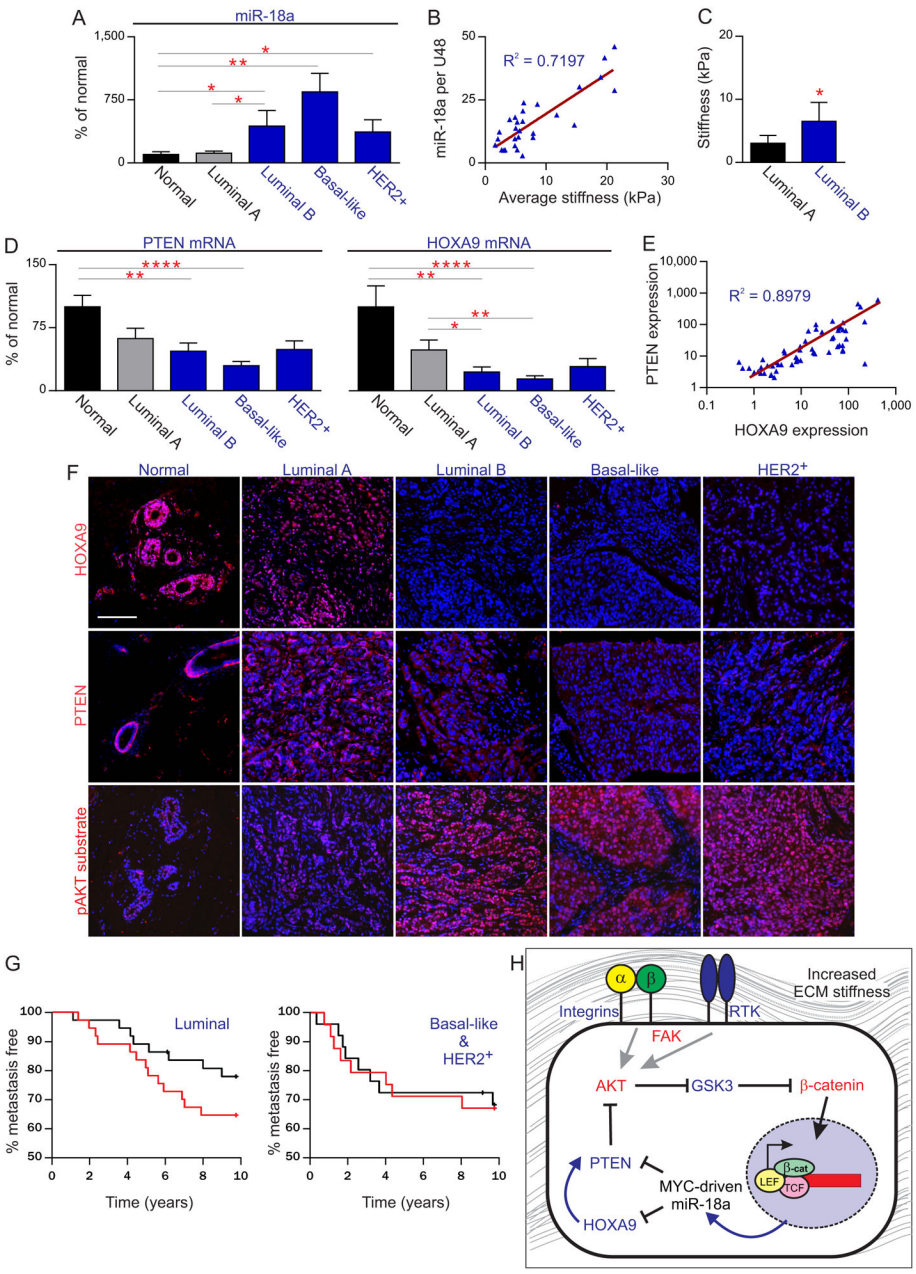

Figure 6. Breast malignancy associates with increased miR-18a and reduced PTEN expression

A. miR-18a in human non-malignant breast samples (Normal) and breast tumor samples (luminal A, luminal B, basal-like and HER2^{+}). Results are normalized to RNU48 and graphed relative to Normal. B. Correlation between miR-18a expression and elastic modulus (upper quartile) in human patient samples (both non-malignant and tumor samples combined). C. Elastic moduli (upper quartile) for luminal A and luminal B breast tumor samples. D. PTEN (left) and HOXA9 (right) mRNA expressions in human non-malignant breast (Normal) samples and breast tumor samples (luminal A, luminal B, basal-like and HER2+). Results are normalized to 18S and graphed relative to Normal. E. Correlation between HOXA9 and PTEN mRNA levels in human patient samples (both non-malignant

and tumor samples combined). F. HOXA9 (top, red), PTEN (middle, red), pAKT substrate (bottom, red) and DAPI (blue) for human non-malignant breast samples (Normal) and breast tumor samples (luminal A, luminal B, basal-like and HER2+). Scale bar, 100μm. G. Kaplan-Meier graph (left) showing that patients with luminal breast cancers whose tumors expressed the highest miR-18a levels (highest expression quartile; red line) experienced significantly reduced metastasis-free survival compared with patients in the lowest quartile (black line). Kaplan-Meier graph (right) showing patients with basal-like and HER2+ breast cancers whose tumors expressed the highest miR-18a levels (highest expression quartile; red line) and lowest miR-18a levels (black line). H. Graphic depicting a model for suppression of PTEN directly via β-catenin stimulation of MYC-driven miR-18a and indirectly through miR-18a regulation of HOXA9. (*, $P<0.05$; **, $P<0.01$; ***, $P< 0.001$)